

Article

Dynamical Collective Excitations and Entanglement of Two Strongly Correlated Rydberg Superatoms

Dong Yan ^{1,*}, Wenjie Bai ¹, Jiannan Bai ¹, Li Chen ¹, Haiyan Han ¹ and Jinhui Wu ²

¹ School of Science and Key Laboratory of Materials Design and Quantum Simulation, Changchun University, Changchun 130022, China; baiwj@mails.ccu.edu.cn (W.B.); baijn@mails.ccu.edu.cn (J.B.); chenl82@ccu.edu.cn (L.C.); hanhy@ccu.edu.cn (H.H.)

² Center for Quantum Sciences and School of Physics, Northeast Normal University, Changchun 130117, China; jhwu@nenu.edu.cn

* Correspondence: yand@ccu.edu.cn

Abstract: Based on the dipole blockade effect and with the aid of the superatom (SA) model, we propose a scheme to investigate the correlated evolution of two Rydberg sub-superatoms (SSAs), formed by two spatially separated atomic Rydberg sub-ensembles but in the same blockade region. Starting from the pure separable states, we investigate the in-phase or anti-phase correlated dynamics and explore how two Rydberg SSAs entangle with each other mediated by a single Rydberg excitation. Starting from the entangled states, we discuss the robustness of the system against decoherence induced by the dephasing rate. Our results show that both the correlated evolution of two Rydberg SSAs and their collective-state entanglement are usually sensitive to the number of each Rydberg SSA. This allows us to coherently manipulate the Rydberg ensemble over long distances from the single-quantum level to the mesoscopic level by changing the number of atoms. Furthermore, the method for dividing an SA into two SSAs and obtaining their spin operators without any approximation can be readily generalized to the case of many SSAs. It may have potential promising applications in quantum information processing and provide an attractive platform to study the quantum-classical correspondence, many-body physics and so on.

Keywords: superatom; dipole blockade; entanglement; correlated evolution



Citation: Yan, D.; Bai, W.; Bai, J.; Chen, L.; Han, H.; Wu, J. Dynamical Collective Excitations and Entanglement of Two Strongly Correlated Rydberg Superatoms. *Photonics* **2022**, *9*, 242. <https://doi.org/10.3390/photonics9040242>

Received: 27 February 2022

Accepted: 31 March 2022

Published: 6 April 2022

Publisher's Note: MDPI stays neutral with regard to jurisdictional claims in published maps and institutional affiliations.



Copyright: © 2022 by the authors. Licensee MDPI, Basel, Switzerland. This article is an open access article distributed under the terms and conditions of the Creative Commons Attribution (CC BY) license (<https://creativecommons.org/licenses/by/4.0/>).

1. Introduction

Due to many exaggerated properties such as very strong interaction between atoms and long lifetime, the neutral Rydberg atom is becoming an extremely attractive platform to build quantum gates in quantum computation [1–8], to realize quantum simulations [9–13], to observe plasma [14–17], etc. It is therefore said that theoretical and experimental investigations with Rydberg atoms are ubiquitous in various aspects of the quantum optics and quantum information. In fact, the basic principles of many applications stem mainly from the idea of dipole blockade effect, in which the strong Rydberg interaction shifts the energy levels of nearby atoms out of resonance when an atom is already in the Rydberg state. As a result, simultaneous excitation of Rydberg ensembles driven by a resonant laser field is inhibited within the so-called blockade region. This enables us to design quantum devices at the level of individual quanta [18–38].

Distance-dependent interaction between Rydberg atoms allows great flexibility in coherent optical control [39,40]. On the one hand, atoms are usually well-localized spatially for precisely controlling the Rydberg interactions. For example, achieving in-phase (anti-phase) dynamics of Rydberg excitations in a bipartite atomic system and entanglement of Rydberg atomic pair in a quadripartite atomic system, where the atoms are neatly arranged in space [41,42]. However on the other hand, without precisely controlling interactions, the quantum information tasks can also be accomplished very well as long as the system enters the rigid Rydberg blockade regime, for example by implementing a mesoscopic

Rydberg gate with a single auxiliary atom and a superatom (SA) [43]. A so-called Rydberg SA is an atomic ensemble that allows for only a single Rydberg excitation shared by whole ensemble within a blockade region. Therefore, it can be used directly to explain the collective phenomena. The level configuration of the Rydberg SA is usually complicated than its elementary atoms except for some special cases, which mainly depends on the energy level of the elementary atom and the laser fields. For example, a Rydberg SA consists of an ensemble of two-level cold atoms in the same blockade region, and can be coherently driven to form an effective two-level configuration by the laser field [44–46]. As a result, it behaves like its elementary atoms, namely a typical absorbing medium. While driving an ensemble of three-level ladder Rydberg atoms into an EIT configure by the coupling field and the probe field, the SA of the same level configuration can be used to simulate this system well only when the probe fields are so weak that only one excitation is populated in the intermediate excited state [47].

Similar to the mean-field method, the Rydberg SA model is becoming a paradigmatic example for studying many-body physics as well, especially for large systems, mainly because the problem of exponentially increasing system size with the particle number can be circumvented to a certain extent. Such a valuable resource has been widely used to explore the novel features caused by the interatomic interaction in the field of quantum optics such as implementation of many-body Rabi oscillations [48], generation or synthesis of collective states [49–51], exploration of Rydberg electromagnetically induced transparency (EIT) [47,52], realization of Rydberg electromagnetically induced grating (EIG) [53,54] and so on. A new physical interface between the collective atomic excitation and optomechanics is initially established by coupling a cavity with a moving membrane to a Rydberg SA [44,55–57], which offers a degree of freedom involving single-photon behavior. Not only is Rydberg SA a powerful tool for fundamental studies of the quantum many-body dynamics, but also plays an important role in application areas. Some work with Rydberg SA has also focused on realizing quantum computation and implementing quantum information tasks [45,58,59] by taking advantage of other merits of Rydberg SA, for example easy manipulation, robustness against the decoherence and excellent scalability. Most interestingly, recent study shows that an SA usually realized via a Rydberg blockade can be regarded as a topologically protected quantum memory. In the regime, the quantum coherence of the subradiant edge state of the SA is robust to random noises. This paves the way to the quantum computation and quantum optics based on topological edge states [46].

In this work, we investigate the correlated evolution of the collective Rydberg excitations and the quantum entanglement between two Rydberg sub-superatoms (SSAs) that formed by two atomic sub-ensembles trapped in two spatially distinct optical dipole traps but in the same blockade region. When the condition of all atoms in the same blockade region is guaranteed, we first reduce the total Hamiltonian of m atoms to a very simple one where only one SA is driven into a two-level configuration by an enhanced Rabi frequency $\sqrt{m}\Omega$ with Ω as the Rabi frequency. Second, to independently manipulate two SSAs, we directly rewrite the effective one-body Hamiltonian according to the collective-state representation and obtain a two-body Hamiltonian. Finally, by solving numerically the two-body Lindblad master equation with varying the single-photon detuning and the numbers of the atoms of two Rydberg SSAs, the correlated evolutions of two SSAs are investigated when the system is prepared in the non-entangled states. The type of the maximal entangled state, as a byproduct of evolution, are determined with the help of the correlated dynamics analysis. We emphasize that dynamical control of in-phase and anti-phase behaviors can be achieved by changing flexibly the number of atoms and the single-photon detuning, from the single-atom level to the mesoscopic level. In addition, we discuss the robustness of the system against the dephasing rate arising from the long-lived Rydberg state and find that the lifetime of different entangled states are all dependent on the number of each SSA. Our results pave the way for coherent manipulation of the strongly coupled systems over long distances, generating mesoscopic entanglement, exploring the classical–quantum correspondence, etc.

2. Model and Equations

As is well known, two Rydberg atoms will undergo strong interaction if they are excited to the high-lying Rydberg state simultaneously. Then the Hamiltonian of an ensemble of m two-level Rydberg atoms driven by a single-mode laser field with frequency ω reads (hereafter we take $\hbar = 1$)

$$\hat{H} = \sum_{j=1}^m \left(\Delta_j \hat{n}_j + \Omega_j \hat{\sigma}_j^+ + \Omega_j \hat{\sigma}_j^- \right) + \sum_{i<j}^m V_{ij} \hat{n}_i \hat{n}_j, \tag{1}$$

where Δ_j is the single-photon detuning of the driving laser from the Rydberg state $|r_j\rangle$. $\hat{n}_j = |r_j\rangle\langle r_j|$ denotes the projection operator to the Rydberg state of an atom at position j and $\hat{\sigma}_j^\pm = |r_j\rangle\langle g_j|$ ($\hat{\sigma}_j^- = |g_j\rangle\langle r_j|$) describes j th atom raising (lowering) operator with the ground state $|g_j\rangle$. The terms Ω_j and V_{ij} account for Rabi frequency of the driving laser field and the vdW coupling strength between two atoms, respectively. Without loss of generality, we focus here on the case of homogeneous coherent coupling, i.e., $\Delta_j = \Delta$ and $\Omega_j = \Omega$.

Driven by a resonant laser field, an ensemble in the same dipole blockade region contains at most one Rydberg excitation due to $\sum_{i<j}^m V_{ij} \rightarrow \infty$. We call this phenomenon the blockade effect. In this case, an ensemble of m two-level Rydberg atoms within the blockade volume can be safely regarded as an SA with two collective states $|G\rangle = |g\rangle^{\otimes m}$ and $|R\rangle = \sum_j^m |g_1, \dots, r_j, \dots, g_m\rangle / \sqrt{m}$. Accordingly, the system can be described by an effective model where the two-level SA is driven by the enhanced laser filled with a Rabi frequency $\sqrt{m}\Omega$. As a result, the quantum dynamics of this system are governed by the effective Hamiltonian

$$\hat{H}_e = -\Delta \hat{N} + \sqrt{m}\Omega (\hat{S}^+ + \hat{S}^-), \tag{2}$$

where $\hat{N} = |R\rangle\langle R|$ and $\hat{S}^\pm = |R\rangle\langle G|$ ($\hat{S}^- = |G\rangle\langle R|$) are the collective projection operator and collective raising (lowering) operator in the superatomic description, respectively.

As shown in Figure 1a, m_l atoms and $m_r = m - m_l$ atoms are trapped in two spatially separated optical dipole traps but keep in the same blockade region. The two sub-ensembles of atoms in respective traps can be regarded as two SSAs. The size of SSA is only determined by the number of atoms in corresponding traps, i.e., the bigger (smaller) SSA we label here refers to the one contains more (less) atoms regardless of the atomic distribution. Each SSA has two collective states $|G_\mu\rangle = |G\rangle^{\otimes m_\mu}$ and $|R_\mu\rangle = \sum_j^{m_\mu} |g_1, \dots, r_j, \dots, g_{m_\mu}\rangle / \sqrt{m_\mu}$ ($\mu = l, r$) (see Figure 1c). According to the definition of the collective states, one can easily establish the relation among them: $|G\rangle = |G_l\rangle|G_r\rangle$ and $|R\rangle = (\sqrt{m_l}|R_l\rangle|G_r\rangle + \sqrt{m_r}|G_l\rangle|R_r\rangle) / \sqrt{m}$. Accordingly, the effective Hamiltonian (2) changes into a two-body Hamiltonian

$$\begin{aligned} \hat{H}_e = & -\frac{\Delta}{m} (m_l \hat{n}_l + m_r \hat{n}_r) \\ & + \Omega [\sqrt{m_l} \hat{\sigma}_l^+ (1 - \hat{n}_r) + \sqrt{m_r} (1 - \hat{n}_l) \hat{\sigma}_r^+ + h.c.] \\ & + \frac{\Delta}{m} (m_l \hat{n}_l \hat{n}_r + m_r \hat{n}_l \hat{n}_r) - \frac{\sqrt{m_l m_r} \Delta}{m} (\hat{\sigma}_l^+ \hat{\sigma}_r^- + \hat{\sigma}_l^- \hat{\sigma}_r^+). \end{aligned} \tag{3}$$

Note that here we have already extracted the collective sub-operators of the left and the right SSAs from the global collective operators of the original SA, i.e., the projection operator $\hat{n}_\mu = |R_\mu\rangle\langle R_\mu|$ and the raising operator $\hat{\sigma}_\mu^+ = |R_\mu\rangle\langle G_\mu|$ ($\mu = l, r$). In Equation (3), the first two lines denote a *not free* Hamiltonian for two SSAs because excitation of one Rydberg SSA depends on the other and they are driven by the laser field with different Rabi frequencies $\sqrt{m_l}(1 - \langle \hat{n}_r \rangle)\Omega$ and $\sqrt{m_r}(1 - \langle \hat{n}_l \rangle)\Omega$, respectively. Here, $\langle \hat{n}_\mu \rangle$ is the mean value of the operator \hat{n}_μ under an arbitrary state. The last line represents a cross blockade and exchange interaction Hamiltonians, respectively. They indicate one SSA excited to its collective Rydberg state blockades the other Rydberg excitation [60,61]. Essentially, the self-blockade interaction between Rydberg atoms in the same blockaded region (see the

final term in Equation (1) has already translated into a cross blockade and an exchange interaction between two SSAs. Undoubtedly, the two SSAs are strongly correlated with each other.

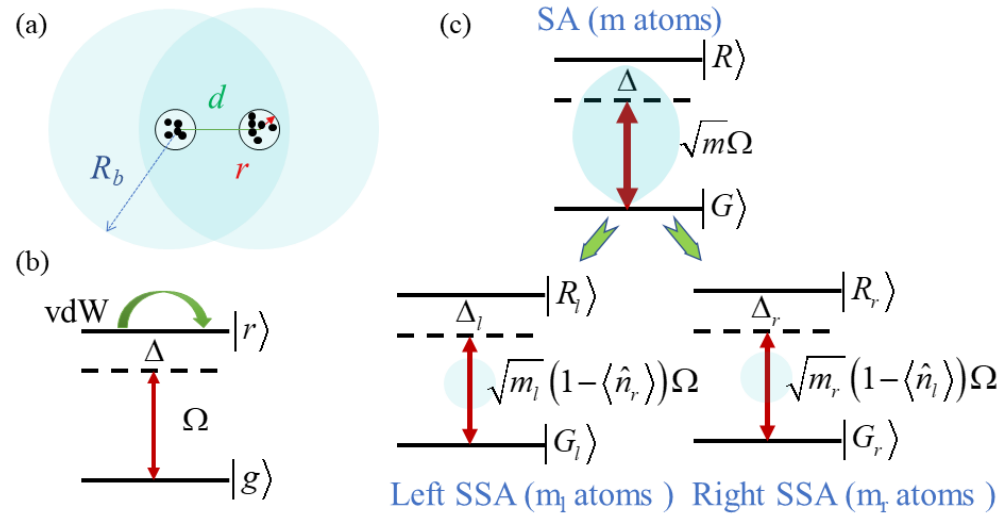


Figure 1. (a) The big (R_b) and the small (r) of the concentric circles denote the borders of the blockade region and the optical dipole trap, respectively. d denotes the distance between two optical dipole traps and $d > r$. The overlap (shading region) of two big circles represents the blockade region for all atoms randomly distributed in two optical dipole traps by setting geometrical parameters to the appropriate values. (b) Level structure for a Rydberg atom. Two atoms with simultaneous Rydberg excitations interact via van der Waals (vdW) potential. (c) Level structures for a SA and its two SSAs: due to the blockade effect, a big SA containing m atoms can be divided into two little ones, i.e., the left SSA and the right one, representing the sub-ensemble of m_l atoms trapped in the left trap and the sub-ensemble of m_r atoms trapped in the right one, respectively.

The dynamical evolution of our system is governed by the two-body Lindblad master equation for density operator ρ

$$\partial_t \rho = -i[\hat{H}_e, \rho] + \mathcal{L}(\rho). \tag{4}$$

Here, $\mathcal{L}(\rho) = L\rho L^\dagger - \frac{1}{2}(\rho L^\dagger L + L^\dagger L\rho)$ describes dissipation processes arising from Rydberg decay rates Γ with $L = \sqrt{\Gamma}(\hat{\sigma}_l^- \otimes I + I \otimes \hat{\sigma}_r^-)$.

The concept of inphase (antiphase), as a basic term in physics, means that two subsystems in composite systems have identical (opposite) dynamic phases. They play the key roles in modern control theory, especially in the study of synchronization. The first anti-phase synchronization can be traced back to the 17th century, Christian Huygens observed a couple of pendulum clocks mounted on the same wooden bar which oscillate in the opposite direction with the same frequency [62]. About two decades ago, the in-phase and anti-phase phenomena of synchronization were already ubiquitous in all areas of natural sciences [63]. Even in the fields of the social sciences, one could find them as well [64]. Up to now, they have led to a wealth of studies in diverse physical platforms, from classical physics [65] to the quantum regime [66–71]. There are two major approaches to quantify the in-phase (anti-phase) evolution between two SSAs: the first is directly estimating the absolute value of the difference of Rydberg excitation probabilities for two subsystems containing exactly the same number of atoms [41] and the second is the Pearson correlation coefficient [72–75], which is usually adopted as a figure of merit to characterize the

phase-matching degree when two subsystems evolve. In our model, for two local Rydberg excitation probabilities $P_l(t)$ and $P_r(t)$, the Pearson correlation coefficient reads

$$C_p = \frac{\int_0^t [P_l(t') - \bar{P}_l][P_r(t') - \bar{P}_r] dt'}{\sqrt{\int_0^t [P_l(t') - \bar{P}_l]^2 dt'} \sqrt{\int_0^t [P_r(t') - \bar{P}_r]^2 dt'}} \tag{5}$$

where $\bar{P}_\mu = \int_0^t P_\mu(t') dt' / t$ ($\mu = l, r$) denotes the time-averaged value of Rydberg excitation probability over the time range from zero to t . The prefect in-phase and anti-phase dynamics are exactly attained at $C_p = 1$ and $C_p = -1$, respectively.

Up to now, a universal entanglement measurement for any quantum system, especially for the high-dimensional systems and the multi-partite systems, has not yet found. However, for two-qubit systems, concurrence is an effective tool to characterize entanglement. As we mentioned above, our system can be translated into a two-qubit system by the collective-state representation; namely, ρ is a 4×4 matrix in the two-superatom basis $\{|G_l\rangle, |R_l\rangle, |G_r\rangle, |R_r\rangle\}$. Therefore, we can use the concurrence to characterize the entanglement between the left SSA and the right one, it reads [76]

$$C(\rho) = \max\{\lambda_1 - \lambda_2 - \lambda_3 - \lambda_4, 0\}, \tag{6}$$

where λ_i ($i = 1, 2, 3, 4$) are the square roots of eigenvalues in decreasing order of the non-Hermitian matrix $\rho(\sigma_y \otimes \sigma_y)\rho^*(\sigma_y \otimes \sigma_y)$. $\sigma_y = \begin{bmatrix} 0 & -i \\ i & 0 \end{bmatrix}$ is a Pauli matrix and ρ^* is the complex conjugate of ρ . The concurrence C varies within the interval $[0, 1]$ such that $C = 0$ denotes no entanglement, while $C = 1$ denotes the maximal entanglement.

3. Results and Discussions

In our work, we adopt the realistic parameters for numerical simulations on temporal evolutions of the local Rydberg excitations, the Pearson correlation coefficient, and the concurrence. Our theoretical model is illustrated in Figure 1b, where levels $|g\rangle$ and $|r\rangle$ are encoded in two states $|5S_{1/2}, F = 2, m_F = 1\rangle$ and $|90S, J = 1/2, m_J = 1/2\rangle$ of cold ^{87}Rb , respectively, with the spontaneous decay rate $\Gamma = 0.02$ MHz, the Rabi frequency $\Omega = 2.0$ MHz, and the vdW coefficient $C_6 \simeq 2\pi \times 1.67 \times 10^{13} \text{ s}^{-1} \mu\text{m}^6$ [41,77]. Then the blockade radius can be obtained by $R_b \simeq [C_6 / \sqrt{\Omega^2 + 4\Delta^2}]^{1/6}$ [78], e.g., $R_b = 11.3 \mu\text{m}$ with $\Delta = 50$ MHz. Furthermore, to guarantee that all atoms trapped in two optical dipole traps are in the same blockade region, as shown in Figure 1a the geometric relation $d + 2r \leq R_b$ must be satisfied. We here choose $d = 5 \mu\text{m}$ and $r = 3 \mu\text{m}$ to meet this condition. Other specific parameters are indicated in respective figure captions if needed.

To demonstrate good reliability and confirm the validity of our approach, we plot in Figure 2 the dynamical evolution of collective Rydberg excitation probabilities based on the original Hamiltonian (1) and the effective two-body Hamiltonian (3) under two kinds of initial states with different numbers of atoms. For simplicity, but without loss of generality, we choose the Rydberg excitation probability P_l of left SSA as our observable to compare. As a result, the calculations based on the two Hamiltonians agree remarkably well with each other. Therefore, we can conclude that the original Hamiltonian can be replaced safely by the effective Hamiltonian with our parameters. Note that, from now on, all numerical simulations are performed based on the effective Hamiltonian and thereby the formidable obstacle that the Hilbert space dimension grows exponentially with the number of particles can be completely removed.

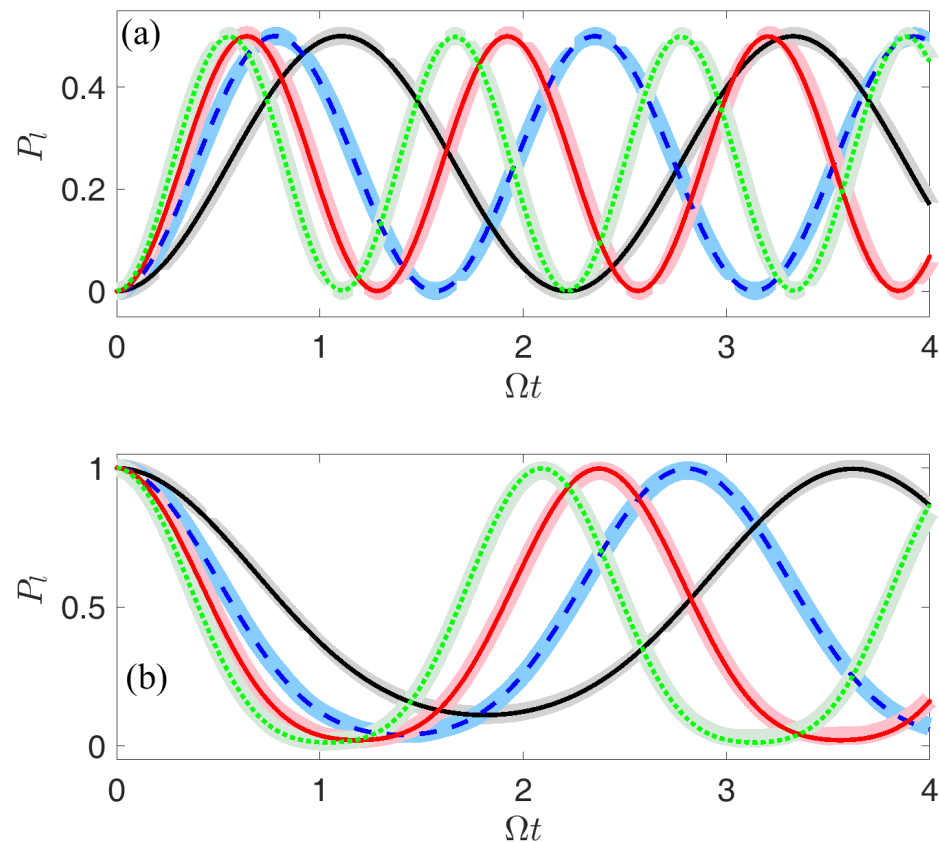


Figure 2. Time evolutions of collective Rydberg excitation probabilities P_l are calculated based on the original Hamiltonian (1) (thick curves) and the effective Hamiltonian (3) (thin curves), respectively. The solid black curve, the dashed blue curve, the dashed–dotted red curve, and the dotted green curve denote the different numbers of atoms (a): $(m_l, m_r) = (1, 1), (2, 2), (3, 3)$ and $(4, 4)$ when the initial state is prepared in $|G_l\rangle|G_r\rangle$ and (b): $(m_l, m_r) = (1, 2), (2, 3), (3, 4)$ and $(4, 5)$ when the initial state is prepared in $|R_l\rangle|G_r\rangle$. Other parameters are given at the beginning of Section 3.

3.1. Time Evolution Starting from the Separable Collective States

In this subsection, we explore how two SSAs entangle with each other mediated by a shared Rydberg excitation in the short-time evolution ($\Omega t = 4$). To this end, we investigate in detail the local collective Rydberg excitations and their correlated behaviors, namely, in-phase or anti-phase time evolution when two SSAs are initially prepared in two kinds of separable (non-entangled) collective states (I): $|G_l\rangle|G_r\rangle$ and (II): $|R_l\rangle|G_r\rangle$.

In case (I), the whole ensemble becomes a nonlocal and homogeneous medium because all the ground-state atoms confined in two traps share equally at most one Rydberg excitation and they can be excited synchronously towards the Rydberg state with equal probabilities whenever the driving field works. Therefore, as shown in Figure 3a1–c1, the bigger the SSA, the higher the collective Rydberg excitation probability. In spite of the difference in size, two SSAs exhibit good in-phase oscillations as manifested by $C_p \equiv 1$ in Figure 3a2–c2. As a result, the left SSA must be in the collective ground state $|G_l\rangle$ as the right one is already in its collective Rydberg state $|R_r\rangle$, and vice versa. Then, the maximally entangled symmetric state $|\psi_+\rangle = (|G_l\rangle|R_r\rangle + |R_l\rangle|G_r\rangle) / \sqrt{2}$, as a byproduct of correlated evolution, can be obtained with two equal-sized SSAs (see Figure 3b2).

When the single-photon detuning is introduced, Figure 3d1 indicates that two Rydberg SSAs always exhibit pretty good in-phase oscillations over the entire time evolution as manifested by $C_p \equiv 1$, regardless of the laser field frequency and the size difference between two SSAs. While Figure 3d2 shows that the maximal concurrence C_{\max} is symmetrical about the single-photon detuning $\Delta = 0$ and the number of the left SSA $m_l = m/2$ (m is even here) and reaches its peak value at $(\Delta, m_l) = (0, m/2)$. The reason is that both single-photon

detuning and the size difference cannot change the nonlocality of the ensemble but can change the collective Rydberg excitation probabilities via weakening the effective Rabi frequency.

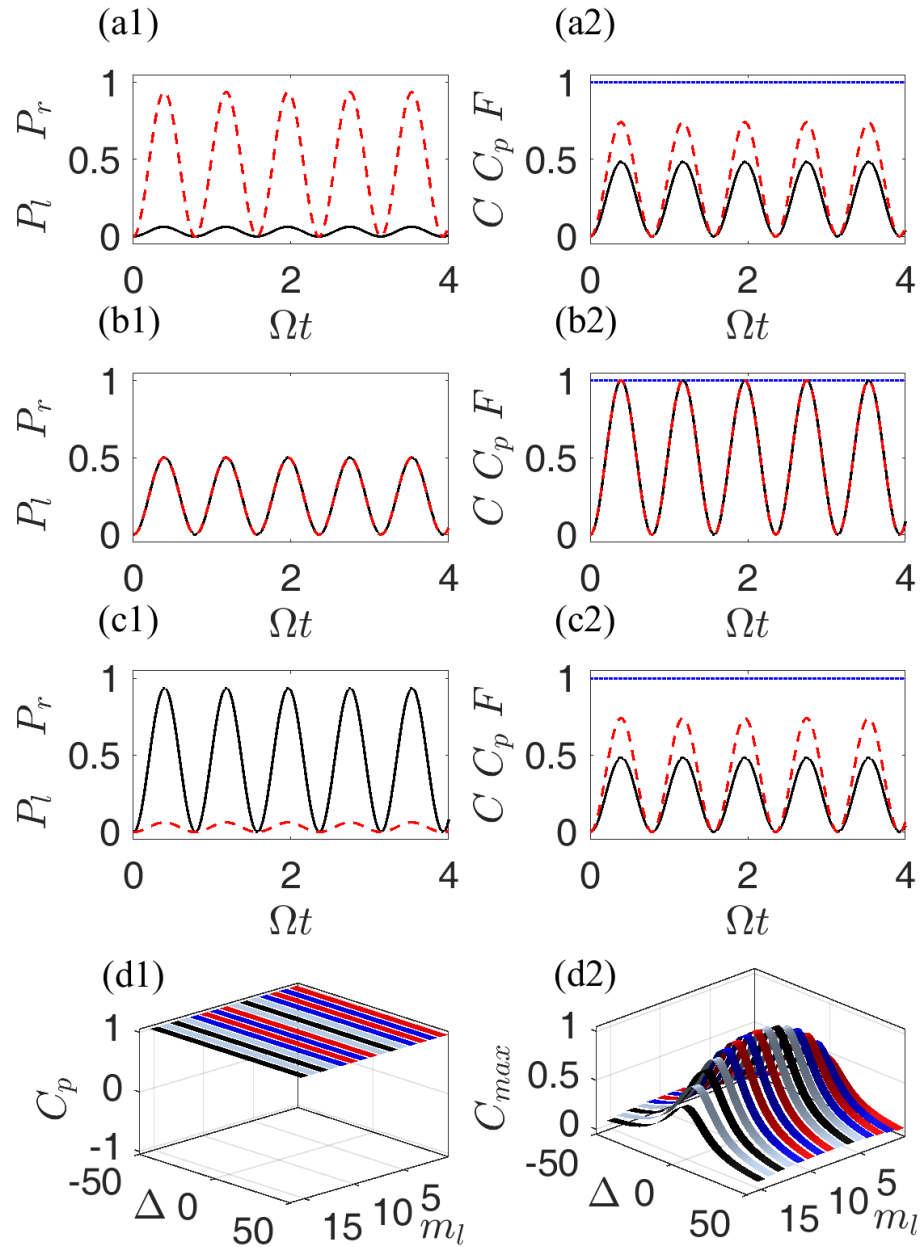


Figure 3. Calculated dynamics for an initial state of $|G_l\rangle|G_r\rangle$. (Left): time evolutions of collective Rydberg excitation probabilities P_l (solid black curve) and P_r (dashed red curve); (right): of the concurrence C (solid black curve), the Pearson correlation coefficient C_p (dotted blue curve), and the fidelity $F_+(t) = |\langle \psi(t) | \psi_+ \rangle|^2$ (dashed red curve) with $|\psi_+\rangle = \frac{1}{\sqrt{2}}(|R_l\rangle|G_r\rangle + |G_l\rangle|R_r\rangle)$ under three sets of parameters (a1,a2): $(m_l, m_r, \Delta) = (1, 15, 0)$; (b1,b2): $(m_l, m_r, \Delta) = (8, 8, 0)$; (c1,c2): $(m_l, m_r, \Delta) = (15, 1, 0)$. Pearson correlation coefficient C_p (d1) and the maximal concurrence C_{max} (d2) as a function of the single-photon detuning Δ and the number of atoms m_l in the left subsuperatom for the evolution time $\Omega t = 4$. The total atom number $m = 16$ remains unchanged. Other parameters are given at the beginning of Section 3.

The correlated dynamics in case (II) are more complicated than the ones in case (I). The main reason is that the time evolution of the system is mostly affected by the pre-existing

collective Rydberg excitation of the left SSA. Naturally, the probability distribution of Rydberg excitation is usually concentrated in the left trap and then the nonlocal homogeneity is broken. In this unbalanced medium, m_l atoms will usually occupy the Rydberg state with higher probability while m_r atoms share the lower Rydberg excitation probability. Specifically, as shown in Figure 4a1–c1 P_r is always less than P_l because $m_l \ll m_r$ while P_r is negligible because $m_l \gg m_r$ for long-time evolution, the equivalence between maximal P_r and P_l can be found only when $m_l = m_r$.

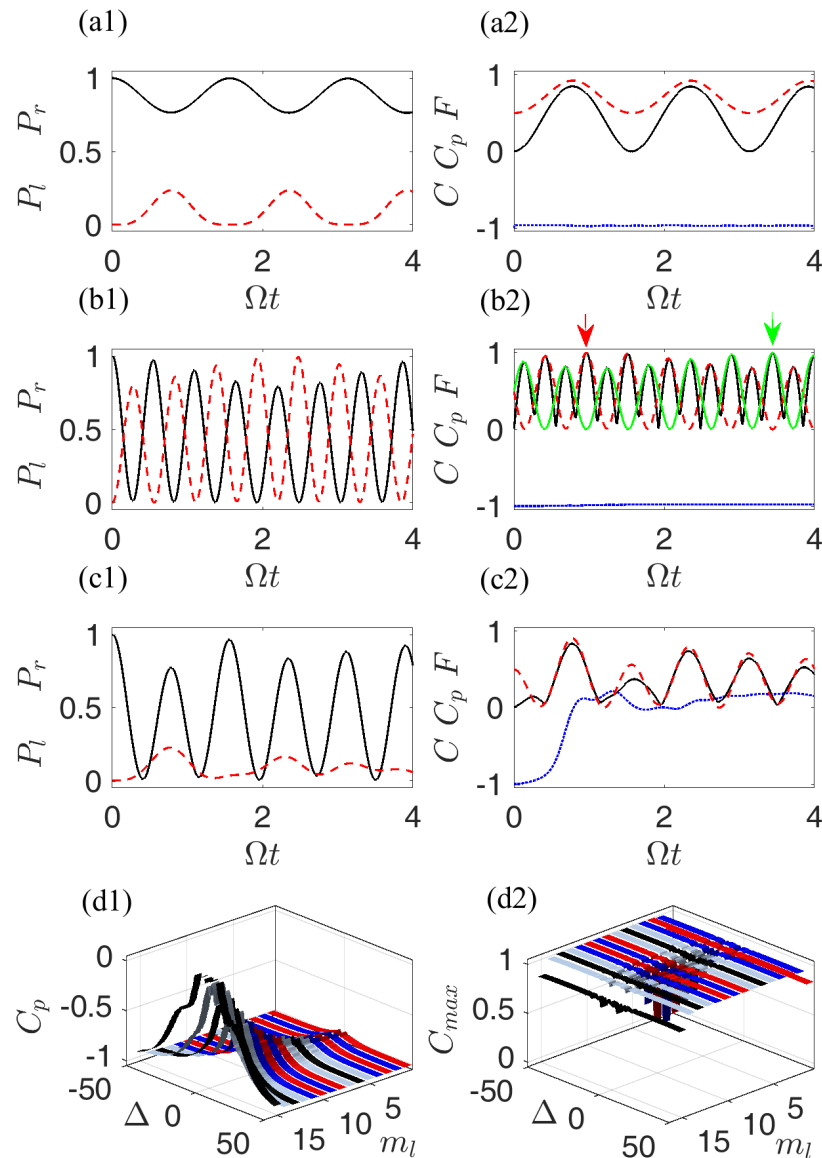


Figure 4. Calculated dynamics for an initial state of $|R_l\rangle|G_r\rangle$. **(Left):** time evolutions of collective Rydberg excitation probabilities P_l (solid black curve) and P_r (dashed red curve); **(right):** of the concurrence C (solid black curve), the Pearson correlation coefficient C_p (dotted blue curve), and the fidelities ($F_-(t)$ is a dashed red curve in **(a2,c2)**, while $f_+(t)$ and $f_-(t)$ are dashed red and dotted green curves in **(b2)**, respectively) under three sets of parameters **(a1,a2):** $(m_l, m_r, \Delta) = (1, 15, 0)$; **(b1,b2):** $(m_l, m_r, \Delta) = (8, 8, 20 \text{ MHz})$; **(c1,c2):** $(m_l, m_r, \Delta) = (15, 1, 2 \text{ MHz})$. Here, $F_-(t) = |\langle \psi(t) | \psi_- \rangle|^2$ with $|\psi_- \rangle = \frac{1}{\sqrt{2}}(|R_l\rangle|G_r\rangle - |G_l\rangle|R_r\rangle)$, while $f_{\pm}(t) = |\langle \psi(t) | \phi_{\pm} \rangle|^2$ with $|\phi_{\pm} \rangle = \frac{1}{\sqrt{2}}(|R_l\rangle|G_r\rangle - e^{\pm i\pi/2}|G_l\rangle|R_r\rangle)$. Pearson correlation coefficient C_p **(d1)** and the maximal concurrence C_{max} **(d2)** as a function of the single-photon detuning Δ and the number of atoms m_l in the left subsuperatom for the evolution time $\Omega t = 4$. The total atom number $m = 16$ remains unchanged. Other parameters are given at the beginning of Section 3.

When the initial state is $|R_l\rangle|G_r\rangle$, the correlated evolution of two SSAs is essentially anti-phase because the left SSA must be deexcited and then the right one is excited whenever the driving field works, they repeatedly exchange at most one Rydberg excitation. However, the correlated dynamics is not uniform throughout the course of time evolution. Specifically, in the first two cases (see Figure 4a1,b1), during the entire time evolution two SSAs exhibit a pretty anti-phase oscillation as manifested by $C_p(t) \equiv -1$ in Figure 4a2,b2. Meanwhile, in the last case, two SSAs exhibit an approximate anti-phase oscillation before $\Omega t = 0.3$ and after that they are nearly uncorrelated as manifested $C_p(t): -1 \rightarrow 0$ in Figure 4c1. This transition again indicates that the global nonlocality is mainly dominated not by $|G_r\rangle$ (P_r vanishes here) but by $|R_l\rangle$. As a result, in the first two cases the maximally entangled asymmetric state $|\psi_{-}\rangle = (|R_l\rangle|G_r\rangle - |G_l\rangle|R_r\rangle)/\sqrt{2}$ and the maximally entangled states $|\phi_{\pm}\rangle = (|R_l\rangle|G_r\rangle - e^{\pm i\pi/2}|G_l\rangle|R_r\rangle)/\sqrt{2}$ can be obtained, respectively (as indicated with two arrows in Figure 4b2). Note that here $\pm i\pi/2$ arises from the phase accumulated in the collective Rabi oscillation between G_l (G_r) and R_l (R_r). While in the third case, an effective entangled state can not be obtained due to the gradually vanishing correlation between two SSAs, especially for the long-time evolution.

From Figure 4d1 we can find that C_p changes gradually from -1 to 0 with increasing m_l as $\Delta = 0$. This demonstrates once again that the correlated dynamics between two SSAs mentioned above are sensitive to the number of atoms of each SSA and the single-photon detuning. Figure 4d2 shows that the maximal entangled states can be obtained except for $\Delta = 0$. C_{max} , including the ones in the cases of $(m_l, m_r) = (1, 15)$ and $(m_l, m_r) = (15, 1)$, seems to be unchanged via exchanging m_l and m_r . Though the values of concurrence in the two cases are both slightly less than the ones in other cases, the core physics behind them is rather different. In the former case, the reason for imperfect entanglement is that the initial state $|R_l\rangle = |r\rangle$ is a completely separable state, which will partly degrade the quantum correlation as the system evolves. While in the latter, the reason is that two SSAs are uncorrelated and the then quantum entanglement will vanish quickly for a longer time, e.g., $\Omega t = 20$ (see also the tendency of relevant curves in Figure 4c2).

3.2. Time Evolution Starting from the Entangled Collective States

In this subsection, we further investigate the correlated dynamics of two SSAs and the robustness of the entangled states against the decay rate when the initial states are prepared in the entangled states $|\psi_{\pm}\rangle = \frac{1}{\sqrt{2}}(|G_l\rangle|R_r\rangle \pm |R_l\rangle|G_r\rangle)$.

Essentially, the entangled symmetric state $|\psi_{+}\rangle$ may serve as the result of the in-phase evolution, namely, simultaneous excitation and deexcitation. When system starts from $|\psi_{+}\rangle$, the initial evolution is usually dominated by the in-phase feature. However, in this time two SSAs can not be excited simultaneously towards the collective Rydberg state but the collective ground state due to the blockade effect, namely, $P_l + P_r \leq 1$. As shown in Figure 5b1, P_l and P_r decrease simultaneously from $P_l = P_r = 0.5$ and keep pretty in-phase oscillation as manifested by $C_p = 1$ during the entire time evolution as $m_l = m_r$. However, as $m_l \neq m_r$ their correlated evolution switches from the in-phase dynamics ($C_p = 1$) to the partially anti-phase dynamics ($C_p = -0.5$) when crossing the critical time $\Omega t = 0.8$ (see Figure 5a1,c1). Obviously, their dynamical phase shift originates from the difference of m_l and m_r , that will affect the respective effective Rabi frequencies two SSAs experienced (see Equation (3)). Figure 5d1 offers much richer physics, e.g., the correlated dynamics can change from a pretty in-phase dynamics ($m_l = m_r$) to an absolute anti-phase dynamics ($m_l \neq m_r$) usually with certain single photon detuning.

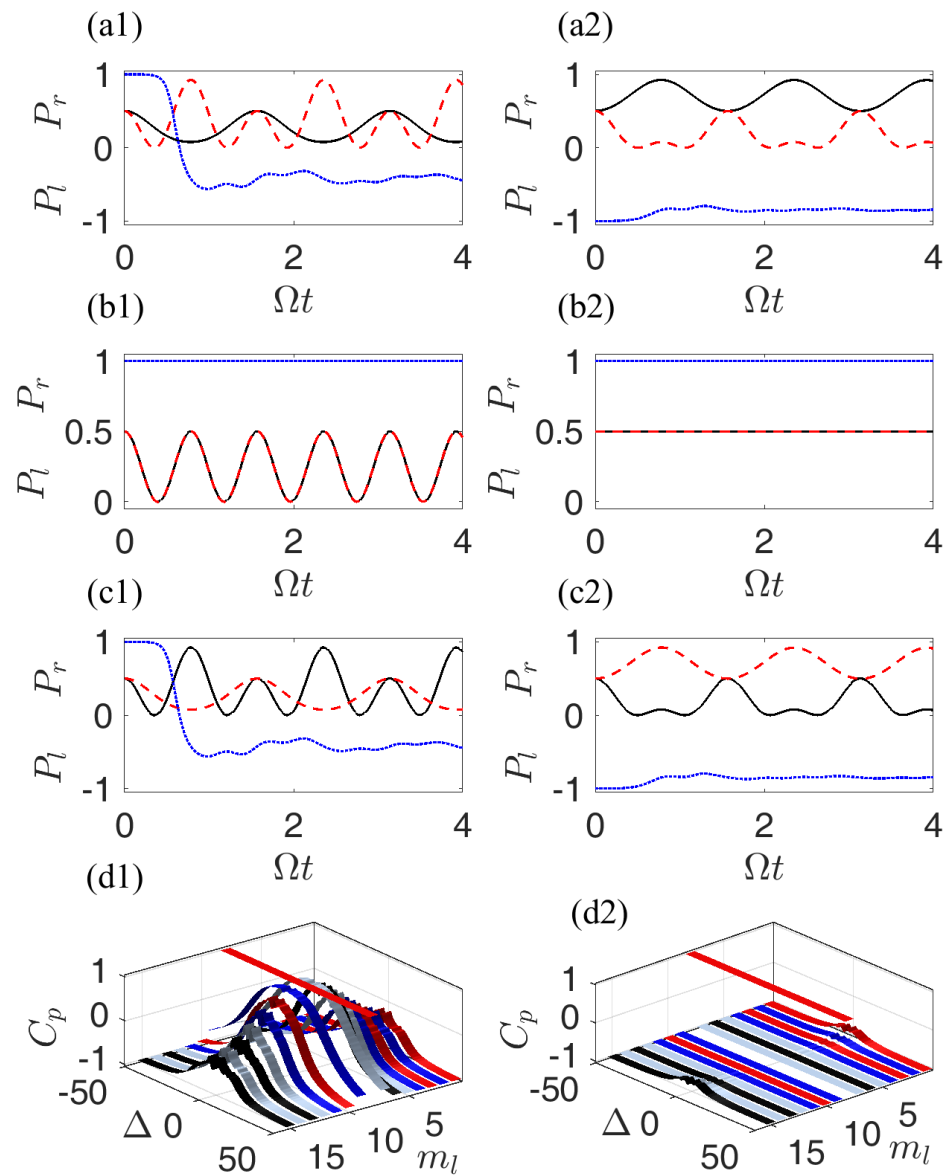


Figure 5. Calculated dynamics for the initial states of $|\psi_+\rangle$ (left column) and $|\psi_-\rangle$ (right column), respectively. Time evolutions of collective Rydberg excitation probabilities P_l (solid black curve), P_r (dashed red curve) and Pearson correlation coefficient C_p (dotted blue curve) under three sets of parameters: **(a1,a2)** $(m_l, m_r) = (1, 15)$; **(b1,b2)** $(m_l, m_r) = (8, 8)$; **(c1,c2)** $(m_l, m_r) = (15, 1)$; **(d1,d2)** Pearson correlation coefficient C_p as a function of the single-photon detuning Δ and the number of atoms m_l with total atom number $m = 16$ for the evolution time $\Omega t = 4$ in the last row. Other parameters are given at the beginning of Section 3.

Similarly to the case of $|\psi_+\rangle$, Figure 5a2,c2 show that two SSAs naturally exhibit an anti-phase oscillation because the system prepared is the entangled asymmetric state $|\psi_-\rangle$ which is regarded as the result of the anti-phase evolution. Due to $m_l \neq m_r$, the Pearson correlation coefficient slightly deviates from the ideal value $C_p = -1$. When $m_l = m_r$, P_l and P_r remain unchanged as also manifested by $C_p = 1$ during the entire time evolution. The reason for this kind of non-trivial behavior is that the system is initially prepared in its dark state $|\psi_-\rangle$ (zero eigenvalue state of the system Hamiltonian (3)), which is only affected by the negligible decay rate γ from the Rydberg state as system evolves. Figure 5d2 shows that all but one exhibit anti-phase correlated dynamics because there is only one dark state, namely the case of $m_l = m_r$.

We finally discuss the decoherence process induced by the dephasing rate from the collective Rydberg state. To this end, we enlarge the evolution time to $\Omega t = 12$ because the dephasing rate is very small. As shown in Figure 6a1,a2, the concurrence C decreases linearly at a speed γt only in the case of $m_l = m_r$ for $|\psi_-\rangle$, while gradually decreasing in an oscillatory manner in other cases. This is demonstrated again in that $|\psi_-\rangle$ is the dark state of the system. Figure 5b1,b2 shows that the concurrence is sensitive to the number of the left SSA and is symmetric with respect to $m_l = m/2$. This is because the effective Rabi frequencies for two SAAs remain unchanged when m_l and m_r are exchanged (see Equation (3)). In addition, the robustness of the system when the system is initially prepared in the entangled symmetric state, ψ_+ is generally higher than the one when the system is initially prepared in the entangled asymmetric state ψ_- . We understand that the anti-phase dynamics, i.e., one SSA, is excited while the other is deexcited simultaneously, canceling partially the coherence in analogy to the EIT.

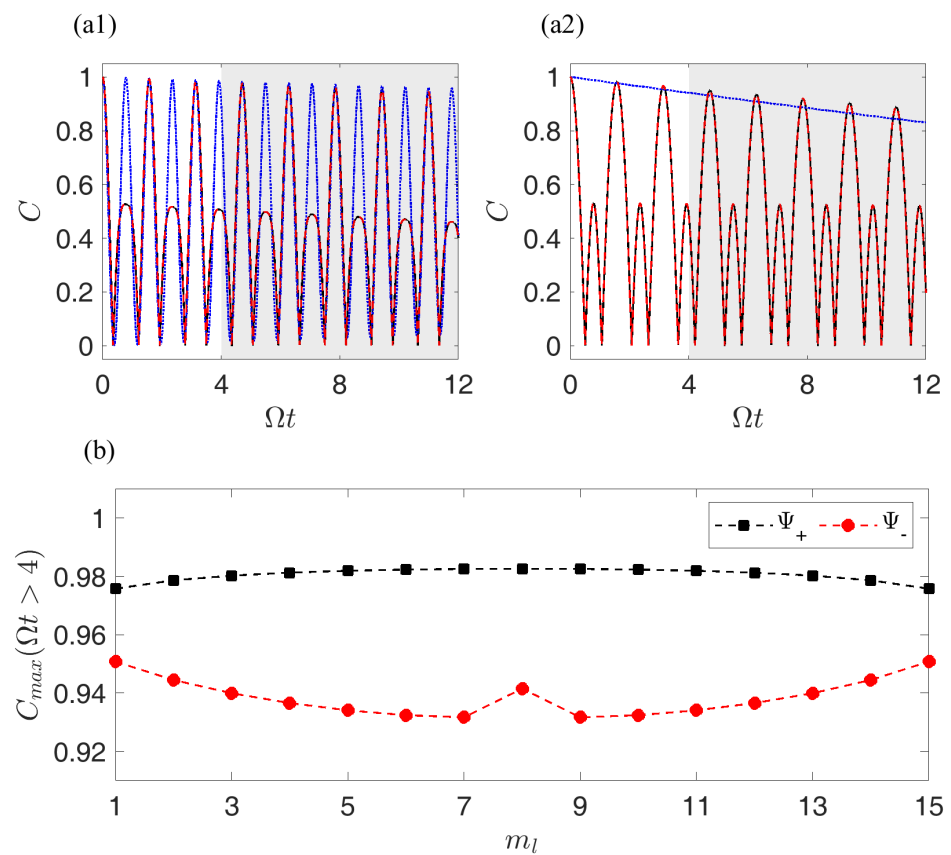


Figure 6. Calculated dynamics for the initial states of $|\psi_+\rangle$ (a1) and $|\psi_-\rangle$ (a2), respectively. Time evolutions of concurrence C . The solid black, the dotted blue, and the dashed red curves correspond to the parameters: $(m_l, m_r) = (1, 15)$, $(m_l, m_r) = (8, 8)$, and $(m_l, m_r) = (15, 1)$. (b) Maximal concurrence C_{max} as a function of the number of atoms m_l with total atom number $n=16$ for the evolution time $12 > \Omega t > 4$ (as indicated with shading region in Figure 6a1,a2). The initial states are $|\psi_+\rangle$ (black squares) and $|\psi_-\rangle$ (red circles), respectively. Other parameters are given at the beginning of Section 3.

4. Conclusions

In summary, we studied the correlated evolution and the quantum entanglement of two strongly correlated Rydberg SSAs, which are Rydberg atomic ensembles trapped in two optical traps but in the same dipole blockade region. When the system is initially prepared, two kinds of pure non-entangled state, the in-phase and anti-phase correlated dynamics between two Rydberg SAAs are investigated. As a byproduct of correlation evolution, the maximally entangled states are obtained and their types can be confirmed in terms of the correlated dynamics. When the system evolves starting from two kinds of

entangled states, the process of decoherence are very different. The correlated dynamics and the lifetime of the collective–time entanglement sensitive to the number of atoms are found. Our results pave the way for coherent manipulation of the strongly coupled systems over long distances, generating mesoscopic entanglement, exploring the classical–quantum correspondence, etc.

Author Contributions: Conceptualization, D.Y. and W.B.; methodology, J.B.; formal analysis, L.C. and D.Y.; writing—original draft preparation, D.Y. and H.H.; writing—review and editing, D.Y. and J.W. All authors have read and agreed to the published version of the manuscript.

Funding: This research was funded by National Natural Science Foundation of China (Grant Nos. 11874004, 12074061, 11204019), Science Foundation of Education Department of Jilin Province (Grant No. JJKH20200557KJ), Nature Science Foundation of Science and Technology Department of Jilin Province (Grant No. 20210101411JC).

Institutional Review Board Statement: Not applicable.

Informed Consent Statement: Not applicable.

Data Availability Statement: Not applicable.

Conflicts of Interest: The authors declare no conflict of interest.

References

- Jaksch, D.; Cirac, J.I.; Zoller, P.; Rolston, S.L.; Côté, R.; Lukin, M.D. Fast Quantum Gates for Neutral Atoms. *Phys. Rev. Lett.* **2000**, *85*, 2208–2210. [[CrossRef](#)] [[PubMed](#)]
- Lukin, M.D.; Fleischhauer, M.; Côté, R.; Duan, L.M.; Jaksch, D.; Cirac, J.I.; Zoller, P. Dipole Blockade and Quantum Information Processing in Mesoscopic Atomic Ensembles. *Phys. Rev. Lett.* **2001**, *87*, 37901. [[CrossRef](#)] [[PubMed](#)]
- Protsenko, I.E.; Raymond, G.; Schlosser, N.; Grangier, P. Operation of a quantum phase gate using neutral atoms in microscopic dipole traps. *Phys. Rev. A* **2002**, *65*, 52301. [[CrossRef](#)]
- Brion, E.; Mølmer, K.; Saffman, M. Quantum Computing with Collective Ensembles of Multilevel Systems. *Phys. Rev. Lett.* **2007**, *99*, 260501. [[CrossRef](#)]
- Wu, H.Z.; Yang, Z.B.; Zheng, S.B. Implementation of a multiqubit quantum phase gate in a neutral atomic ensemble via the asymmetric Rydberg blockade. *Phys. Rev. A* **2010**, *82*, 34307. [[CrossRef](#)]
- Wu, H.; Huang, X.-R.; Hu, C.-S.; Yang, Z.-B.; Zheng, S.-B. Rydberg-interaction gates via adiabatic passage and phase control of driving fields. *Phys. Rev. A* **2017**, *96*, 22321. [[CrossRef](#)]
- Shi, X.-F. Deutsch, Toffoli, and CNOT Gates via Rydberg Blockade of Neutral Atoms. *Phys. Rev. Appl.* **2018**, *9*, 51001. [[CrossRef](#)]
- Wu, J.-L.; Wang, Y.; Han, J.-X.; Su, S.-L.; Xia, Y.; Jiang, Y.Y.; Song, J. Resilient quantum gates on periodically driven Rydberg atoms. *Phys. Rev. A* **2021**, *103*, 12601. [[CrossRef](#)]
- Weimer, H.; Müller, M.; Lesanovsky, I.; Zoller, P.; Büchler, H.P. A Rydberg quantum simulator. *Nat. Phys.* **2010**, *6*, 382–388. [[CrossRef](#)]
- Labuhn, H.; Barredo, D.; Ravets, S.; de Léséleuc, S.; Macrì, T.; Lahaye, T.; Browaeys, A. Tunable two-dimensional arrays of single Rydberg atoms for realizing quantum Ising models. *Nature* **2016**, *534*, 667–670. [[CrossRef](#)]
- Bernien, H.; Schwartz, S.; Keesling, A.; Levine, H.; Omran, A.; Pichler, H.; Choi, S.; Zibrov, A.S.; Endres, M.; Greiner, M.; et al. Probing many-body dynamics on a 51-atom quantum simulator. *Nature* **2017**, *551*, 579–584. [[CrossRef](#)] [[PubMed](#)]
- Barredo, D.; Lienhard, V.; de Léséleuc, S.; Lahaye, T.; Browaeys, A. Synthetic three-dimensional atomic structures assembled atom by atom. *Nature* **2018**, *561*, 79–82. [[CrossRef](#)] [[PubMed](#)]
- Kim, H.; Park, Y.J.; Kim, K.; Sim, H.-S.; Ahn, J. Detailed Balance of Thermalization Dynamics in Rydberg-Atom Quantum Simulators. *Phys. Rev. Lett.* **2018**, *120*, 180502. [[CrossRef](#)]
- Robinson, M.P.; Laburthe-Tolra, B.; Noel, M.W.; Gallagher, T.F.; Pillet, P. Spontaneous Evolution of Rydberg Atoms into an Ultracold Plasma. *Phys. Rev. Lett.* **2000**, *85*, 4466. [[CrossRef](#)] [[PubMed](#)]
- Bannasch, G.; Pohl, T. Rydberg-atom formation in strongly correlated ultracold plasmas. *Phys. Rev. A* **2011**, *84*, 52710. [[CrossRef](#)]
- Bannasch, G.; Killian, T.C.; Pohl, T. Strongly Coupled Plasmas via Rydberg Blockade of Cold Atoms. *Phys. Rev. Lett.* **2013**, *110*, 253003. [[CrossRef](#)]
- Robert-de-Saint-Vincent, M.; Hofmann, C.S.; Schempp, H.; Günter, G.; Whitlock, S.; Weidemüller, M. Spontaneous Avalanche Ionization of a Strongly Blockaded Rydberg Gas. *Phys. Rev. Lett.* **2013**, *110*, 45004. [[CrossRef](#)]
- Firstenberg, O.; Adams, C.S.; Hofferber, S. Nonlinear quantum optics mediated by Rydberg interactions. *J. Phys. B At. Mol. Opt. Phys.* **2016**, *49*, 152003. [[CrossRef](#)]
- Liang, Q.-Y.; Venkatramani, A.V.; Cantu, S.H.; Nicholson, T.L.; Gullans, M.J.; Gorshkov, A.V.; Thompson, J.D.; Chin, C.; Lukin, M.D.; Vuletic, V. Observation of three-photon bound states in a quantum nonlinear medium. *Science* **2018**, *359*, 783–786. [[CrossRef](#)]

20. Labuhn, H.; Ravets, S.; Barredo, D.; Béguin, L.; Nogrette, F.; Lahaye, T.; Browaeys, A. Single-atom addressing in microtraps for quantum-state engineering using Rydberg atoms. *Phys. Rev. A* **2014**, *90*, 23415. [[CrossRef](#)]
21. Petrosyan, D.; Bhaktavatsala Rao, D.D.; Mølmer, K. Filtering single atoms from Rydberg-blockaded mesoscopic ensembles. *Phys. Rev. A* **2015**, *91*, 43402. [[CrossRef](#)]
22. Saffman, M.; Walker, T.G. Creating single-atom and single-photon sources from entangled atomic ensembles. *Phys. Rev. A* **2002**, *66*, 65403. [[CrossRef](#)]
23. Walker, T.G. Strongly interacting photons. *Nature* **2012**, *488*, 39–40. [[CrossRef](#)]
24. Müller, M.; Kölle, A.; Löw, R.; Pfau, T.; Calarco, T.; Montangero, S. Room-temperature Rydberg single-photon source. *Phys. Rev. A* **2013**, *87*, 53412. [[CrossRef](#)]
25. Dudin, Y.O.; Kuzmich, A. Strongly Interacting Rydberg Excitations of a Cold Atomic Gas. *Science* **2012**, *336*, 887–889. [[CrossRef](#)] [[PubMed](#)]
26. Maxwell, D.; Szwer, D.J.; Paredes-Barato, D.; Busche, H.; Pritchard, J.D.; Gauguier, A.; Weatherill, K.J.; Jones, M.P.A.; Adams, C.S. Storage and Control of Optical Photons Using Rydberg Polaritons. *Phys. Rev. Lett.* **2013**, *110*, 103001. [[CrossRef](#)]
27. Peyronel, T.; Firstenberg, O.; Liang, Q.-Y.; Hofferberth, S.; Gorshkov, A.V.; Pohl, T.; Lukin, M.D.; Vuletic, V. Quantum nonlinear optics with single photons enabled by strongly interacting atoms. *Nature* **2012**, *488*, 57–60. [[CrossRef](#)]
28. Gorshkov, A.V.; Nath, R.; Pohl, T. Dissipative Many-Body Quantum Optics in Rydberg Media. *Phys. Rev. Lett.* **2013**, *110*, 153601. [[CrossRef](#)]
29. Honer, J.; Löw, R.; Weimer, H.; Pfau, T.; Büchler, H.P. Artificial Atoms Can Do More Than Atoms: Deterministic Single Photon Subtraction from Arbitrary Light Fields. *Phys. Rev. Lett.* **2011**, *107*, 93601. [[CrossRef](#)]
30. Gorshkov, A.V.; Otterbach, J.; Fleischhauer, M.; Pohl, T.; Lukin, M.D. Photon-Photon Interactions via Rydberg Blockade. *Phys. Rev. Lett.* **2011**, *107*, 133602. [[CrossRef](#)]
31. Gorniaczyk, H.; Tresp, C.; Schmidt, J.; Fedder, H.; Hofferberth, S. Single-Photon Transistor Mediated by Interstate Rydberg Interactions. *Phys. Rev. Lett.* **2014**, *113*, 53601. [[CrossRef](#)] [[PubMed](#)]
32. Tiarks, D.; Baur, S.; Schneider, K.; Dürr, S.; Rempe, G. Single-Photon Transistor Using a Förster Resonance. *Phys. Rev. Lett.* **2014**, *113*, 53602.
33. Chen, W.; Beck, K.M.; Bücker, R.; Gullans, M.; Lukin, M.D.; Tanji-Suzuki, H.; Vuletić, V. All-Optical Switch and Transistor Gated by One Stored Photon. *Science* **2013**, *341*, 768–770. [[CrossRef](#)] [[PubMed](#)]
34. Baur, S.; Tiarks, D.; Rempe, G.; Dürr, S. Single-Photon Switch Based on Rydberg Blockade. *Phys. Rev. Lett.* **2014**, *112*, 73901. [[CrossRef](#)]
35. Tresp, C.; Zimmer, C.; Mirgorodskiy, I.; Gorniaczyk, H.A. Single-Photon Absorber Based on Strongly Interacting Rydberg Atoms. *Phys. Rev. Lett.* **2016**, *117*, 223001. [[CrossRef](#)]
36. Friedler, I.; Kurizki, G.; Petrosyan, D. Deterministic quantum logic with photons via optically induced photonic band gaps. *Phys. Rev. A* **2005**, *71*, 23803. [[CrossRef](#)]
37. Paredes-Barato, D.; Adams, C.S. All-Optical Quantum Information Processing Using Rydberg Gates. *Phys. Rev. Lett.* **2014**, *112*, 40501. [[CrossRef](#)]
38. Yu, D. Single-photon emitter based on an ensemble of lattice-trapped interacting atoms. *Phys. Rev. A* **2014**, *89*, 63809. [[CrossRef](#)]
39. Saffman, M.; Walker, T.G.; Mølmer, K. Quantum information with Rydberg atoms. *Rev. Mod. Phys.* **2010**, *82*, 2313. [[CrossRef](#)]
40. Olmos, B.; Li, W.; Hofferberth, S.; Lesanovsky, I. Amplifying single impurities immersed in a gas of ultracold atoms. *Phys. Rev. A* **2011**, *84*, 41607. [[CrossRef](#)]
41. Fan, C.H.; Zhang, H.X.; Wu, J.H. In-phase and antiphase dynamics of Rydberg atoms with distinguishable resonances. *Phys. Rev. A* **2019**, *99*, 33813. [[CrossRef](#)]
42. Zhang, H.X.; Fan, C.H.; Wu, J.H. In-phase and anti-phase entanglement dynamics of Rydberg atomic pairs. *Opt. Express* **2020**, *28*, 35350–35362. [[CrossRef](#)] [[PubMed](#)]
43. Müller, M.; Lesanovsky, I.; Weimer, H.; Büchler, H.P.; Zoller, P. Mesoscopic Rydberg Gate Based on Electromagnetically Induced Transparency. *Phys. Rev. Lett.* **2009**, *102*, 170502. [[CrossRef](#)]
44. Carmele, A.; Vogell, B.; Stannigel, K.; Zoller, P. Opto-nanomechanics strongly coupled to a Rydberg superatom: Coherent versus incoherent dynamics. *New J. Phys.* **2014**, *16*, 63042. [[CrossRef](#)]
45. Zhao, P.Z.; Wu, X.; Xing, T.H.; Xu, G.F.; Tong, D.M. Nonadiabatic holonomic quantum computation with Rydberg superatoms. *Phys. Rev. A* **2018**, *98*, 32313. [[CrossRef](#)]
46. Nie, W.; Peng, Z.H.; Nori, F.; Liu, Y.-X. Topologically Protected Quantum Coherence in a Superatom. *Phys. Rev. Lett.* **2020**, *124*, 23603. [[CrossRef](#)]
47. Petrosyan, D.; Otterbach, J.; Fleischhauer, M. Electromagnetically Induced Transparency with Rydberg Atoms. *Phys. Rev. Lett.* **2011**, *107*, 213601. [[CrossRef](#)]
48. Stanojevic, J.; Côté, R. Many-body Rabi oscillations of Rydberg excitation in small mesoscopic samples. *Phys. Rev. A* **2009**, *80*, 33418. [[CrossRef](#)]
49. Dür, W.; Vidal, G.; Cirac, J.I. Three qubits can be entangled in two inequivalent ways. *Phys. Rev. A* **2000**, *62*, 62314. [[CrossRef](#)]
50. Heidemann, R.; Raitzsch, U.; Bendkowsky, V.; Butscher, B.; Löw, R.; Santos, L.; Pfau, T. Evidence for Coherent Collective Rydberg Excitation in the Strong Blockade Regime. *Phys. Rev. Lett.* **2007**, *99*, 163601. [[CrossRef](#)]

51. Kumar, S.; Sheng, J.T.; Sedlacek, J.A.; Fan, H.Q.; Shaffer, J.P. Collective state synthesis in an optical cavity using Rydberg atom dipole blockade. *J. Phys. B At. Mol. Opt. Phys.* **2016**, *49*, 64014. [[CrossRef](#)]
52. Yan, D.; Liu, Y.-M.; Bao, Q.-Q.; Fu, C.-B.; Wu, J.-H. Electromagnetically induced transparency in an inverted-Y system of interacting cold atoms. *Phys. Rev. A* **2012**, *86*, 23828. [[CrossRef](#)]
53. Liu, Y.-M.; Tian, X.-D.; Wang, X.; Yan, D.; Wu, J.-H. Cooperative nonlinear grating sensitive to light intensity and photon correlation. *Opt. Lett.* **2016**, *41*, 408–411. [[CrossRef](#)] [[PubMed](#)]
54. Asghar, S.; Qamar, Z.S.; Qamar, S. Electromagnetically induced grating with Rydberg atoms. *Phys. Rev. A* **2016**, *94*, 33823. [[CrossRef](#)]
55. Carmele, A.; Qamar, Z.S.; Qamar, S. Strong coupling of a Rydberg superatom to a moving membrane. *Proc. SPIE* **2015**, 9357, 93570S.
56. Bariani, F.; Otterbach, J.; Tan, H.; Meystre, P. Single-atom quantum control of macroscopic mechanical oscillators. *Phys. Rev. A* **2014**, *89*, 11801(R). [[CrossRef](#)]
57. Yan, D.; Wang, Z.-H.; Ren, C.-N.; Gao, H.; Li, Y.; Wu, J.-H. Duality and bistability in an optomechanical cavity coupled to a Rydberg superatom. *Phys. Rev. A* **2015**, *91*, 23813. [[CrossRef](#)]
58. Weber, T.M.; Höning, M.; Niederprüm, T.; Manthey, T.; Thomas, O.; Guarrera, V.; Fleischhauer, M.; Barontini, G.; Ott, H. Mesoscopic Rydberg-blockaded ensembles in the superatom regime and beyond. *Nat. Phys.* **2015**, *11*, 157–161. [[CrossRef](#)]
59. Su, S.-L.; Gao, Y.; Liang, E.J.; Zhang, S. Fast Rydberg antiblockade regime and its applications in quantum logic gates. *Phys. Rev. A* **2017**, *95*, 22319. [[CrossRef](#)]
60. Li, W.B.; Viscor, D.; Hofferberth, S.; Lesanovsky, I. Electromagnetically Induced Transparency in an Entangled Medium. *Phys. Rev. Lett.* **2014**, *112*, 243601. [[CrossRef](#)]
61. Liu, Y.-M.; Tian, X.-D.; Yan, D.; Zhang, Y.; Cui, C.-L.; Wu, J.-H. Nonlinear modifications of photon correlations via controlled single and double Rydberg blockade. *Phys. Rev. A* **2015**, *91*, 43802. [[CrossRef](#)]
62. Huygens, C. *Horologium Oscillatorium*; F. Muguet: Paris, France, 1673.
63. Pikovsky, A.S.; Rosenblum, M.; Kurths, J. *Synchronization: A Universal Concept in Nonlinear Science*; Cambridge University Press: New York, NY, USA, 2001.
64. Osipov, G.V.; Kurths, J.; Zhou, C. *Synchronization in Oscillatory Networks*; Springer Series in Synergetics; Springer: Berlin/Heidelberg, Germany, 2007.
65. Acebrón, J.A.; Bonilla, L.L.; Pérez Vicente, C.J.; Ritort, F.; Spigler, R. The Kuramoto model: A simple paradigm for synchronization phenomena. *Rev. Mod. Phys.* **2005**, *77*, 137. [[CrossRef](#)]
66. Lee, T.E.; Sadeghpour, H.R. Quantum Synchronization of Quantum van der Pol Oscillators with Trapped Ions. *Phys. Rev. Lett.* **2013**, *111*, 234101. [[CrossRef](#)]
67. Walter, S.; Nunnenkamp, A.; Bruder, C. Quantum synchronization of two Van der Pol oscillators. *Ann. Phys.* **2015**, *527*, 131. [[CrossRef](#)]
68. Giorgi, G.L.; Galve, F.; Zambrini, R. Probing the spectral density of a dissipative qubit via quantum synchronization. *Phys. Rev. A* **2016**, *94*, 52121. [[CrossRef](#)]
69. Roulet, A.; Bruder, C. Synchronizing the Smallest Possible System. *Phys. Rev. Lett.* **2018**, *121*, 53601. [[CrossRef](#)] [[PubMed](#)]
70. Hillbrand, J.; Auth, D.; Piccardo, M.; Opačak, N.; Gornik, E.; Strasser, G.; Capasso, F.; Breuer, S.; Schwarz, B. In-Phase and Anti-Phase Synchronization in a Laser Frequency Comb. *Phys. Rev. Lett.* **2020**, *124*, 23901. [[CrossRef](#)]
71. Parra-López, Á.; Bergli, J. Synchronization in two-level quantum systems. *Phys. Rev. A* **2020**, *101*, 62104. [[CrossRef](#)]
72. Bellomo, B.; Giorgi, G.L.; Palma, G.M.; Zambrini, R. Quantum synchronization as a local signature of super- and subradiance. *Phys. Rev. A* **2017**, *95*, 43807. [[CrossRef](#)]
73. Karpat, G.; Yaçınkaya, İ.; Çakmak, B. Quantum synchronization in a collision model. *Phys. Rev. A* **2019**, *100*, 12133. [[CrossRef](#)]
74. Karpat, G.; Yaçınkaya, İ.; Çakmak, B. Quantum synchronization of few-body systems under collective dissipation. *Phys. Rev. A* **2020**, *101*, 42121. [[CrossRef](#)]
75. Jebarathinam, C.; Home, D.; Sinha, U. Pearson correlation coefficient as a measure for certifying and quantifying high-dimensional entanglement. *Phys. Rev. A* **2020**, *101*, 22112. [[CrossRef](#)]
76. Wootters, W.K. Entanglement of Formation of an Arbitrary State of Two Qubits. *Phys. Rev. Lett.* **1998**, *80*, 2245. [[CrossRef](#)]
77. Singer, K.; Stanojevic, J.; Weidemüller, M.; Côté, R. Long-range interactions between alkali Rydberg atom pairs correlated to the ns-ns, np-np and nd-nd asymptotes. *J. Phys. B At. Mol. Opt. Phys.* **2005**, *38*, S295. [[CrossRef](#)]
78. Balewski, J.B.; Krupp, A.T.; Gaj, A.; Hofferberth, S.; Löw, R.; Pfau, T. Rydberg dressing: Understanding of collective many-body effects and implications for experiments. *New J. Phys.* **2014**, *16*, 63012. [[CrossRef](#)]